CLAWAR 2014 – Proceedings of the Seventeenth International Conference on Climbing and Walking Robots and the Support Technologies for Mobile Machines, Poznan, Poland, 21 – 23 July 2014

Modeling and simulation of a silo cleaning robot

K. Dandan* A. Ananiev and I. Kalaykov
AASS, Örebro University
70182 Örebro, Sweden
* *E-mail: kinan.dandan@oru.se*
www.aass.oru.se

A suspended robot for surface cleaning in silos is presented in this paper. The suggested concept is a reasonable compromise between the basic contradicting factors in the design: small entrance and large surface of the confined space, suspension and stabilization of the robot. A dynamic study for the suspended robot is presented in this paper. A dynamic simulation in MSC ADAMS is carried out to confirm the results from the theoretic study.

Keywords: Suspended robot; Cleaning robot; Dynamic model; Dynamic simulation.

1. Introduction

Cleaning a silo is a tedious work and very dangerous job for humans due to many factors such as: unsafe oxygen level, engulfment, biological, mechanical, electrical, and atmospheric hazards.[4] The requirements of the EU norms related to hygiene and food quality imply that silos should be cleaned more frequently and obligatory after a silo is totally emptied. Therefore, there is an increased societal need of silo cleaning and a natural necessity of replacing humans by robot manipulators in executing this risky job.

A typical food silo has a cylindrical shape with a $20 - 30\ m$ height and $4 - 8\ m$ diameter, with cement surface. The bulk material is fed at the top and taken out at the bottom. Dry cleaning with pressurized air (air jets) is the preferable and recommended cleaning method. There is at least one circular (diameter 80 cm) or rectangular ($80 \times 80\ cm$) inspections hole placed on the silo roof, usually not placed at the central vertical axis of the silo. Today normally humans called "silo-divers" are lowered through this small hole. In addition cleaning instrumentation like air jets connected to air compressor by hose are also lowered along with 1-2 ropes as a backup for the hanging diver and provision of additional tools if needed. The silo-diver

sits on a special suspended on a rope chair and rotates a long-armed air jet around the silo wall. Of course he (no women are reported to exercise this job) is well dressed and equipped with respiratory means.

In a previous work,[2] a detailed overview of the problems in building a robotic solution to substitute humans in silo cleaning was given. It highlighted that none of the existing climbing or walking on walls robots can be used for the purpose, therefore a concept of a suspended robot for surface cleaning in silos (SIRO) was presented (Fig.1). The suggested design appears to be a reasonable compromise between the basic contradicting factors - small entrance and large surface of the confined space. It contains:

- cleaning robot with two platforms - in retracted form on Fig.1(a) and in opened form on Fig.1(b);
- support unit consisting of: (1) control unit for all functions of the system; (2) lifting arm for positioning the cleaning robot at the silo central axis and spools of steel cables with respective driving motors used for robot suspension and motion; (3) steel cables coming from the support unit through the lifting arm to the robot platforms;
- cleaning tools attached to the center of the platform (not shown on the figures) which rotate around the platform center.

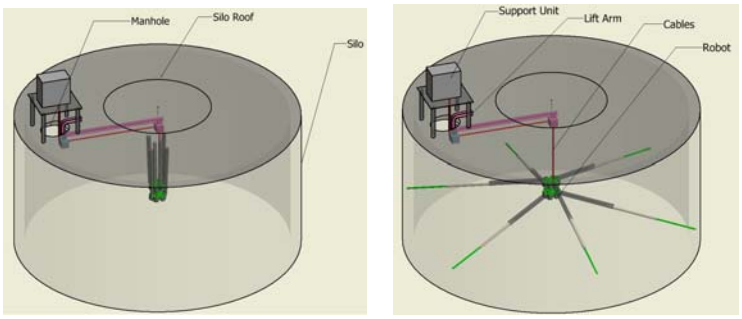

(a) The initial pose (b) The working pose

Fig. 1. The proposed SIRO cleaning robot inside a silo

In fact SIRO is a double pendulum consisting of two parts - a normal naturally stable pendulum and a naturally unstable pendulum attached at the end of the first one, Fig.1(a). The combination of stable and unstable part does not guarantee the stability of the entire system. Swinging of the normal pendulum appears always, and mostly at the initial phase just after the robot is allocated at its initial top pose inside the silo. During the transition to the working pose, Fig.1(b), the arms of both platforms

gradually open due to the gravity and this motion modifies the position of the center of mass, the moment of inertia and the angular velocity for the second pendulum that generates undesired and high risky swing. Therefore, in the present work we do dynamical analysis of SIRO for investigating the circumstances of this phenomenon in order to find out the conditions to avoid it. Several papers study the dynamic response and the control of the double pendulum.[1,5] Meanwhile none of them discuss the variable parameters for the second pendulum, which is the case of our robot.

In Section 2 the principle of operation of the SIRO robot is described. Then, in Section 3 we develop a dynamical model using the Euler-Lagrange equation. The real designed robot is simulated in Section 4. The concluding section summarizes the obtained results.

2. Principle of operation

Reaching every point of the silo interior surface is the substantial function for SIRO. To achieve this functionality two movements are used: a translation along the silo's vertical axis and a rotation around that axis.

The robot is transported to the silo roof in folded configuration that is sufficiently small to enter the manhole, Fig. 1(a). Then, after being attached to the suspension and crawling cables, the robot is lowered into the silo by using these cables and the lift arm, which is lowered in the same time.

When the robot takes its highest position inside the silo, all six arms of both platforms are released and they rotate down around their horizontal axes about 100° until reaching full open pose, which is determined by shoulders on the central bodies of the two platforms.

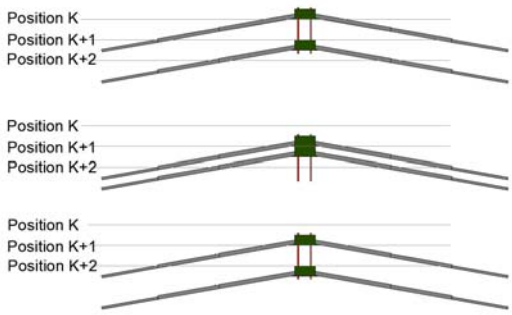

Fig. 2. Crawling movement inside silo space

For holding a vertical position, the three arms of at least one of the top/bottom platforms extend until they get contact to the interior silo surface. The friction force between the arms and the vertical surface must be

bigger than the gravity force depending on the mass of the robot, $F_{friction} > F_{gravity}$. A pushing force F_{push} produced by a ball screw mechanisms in the arms generates an appropriate friction force. Furthermore, the arch shape formed by the robot arms configuration reinforces the stability as well, where the central body of the platform plays the role of a keystone in the arch. At every moment at least one platform should be able to hold robot's weight and prevent vertical sliding.

The movement inside the silo space is achieved by a vertical crawling. The crawling step is determined by the distance between the two platforms, which depends on the area that the cleaning tools have to scan. Crawling is done by small sequential retracting/expanding of the platform arms followed by sequential pull/release of the suspension and crawling cables. Fig. 2 illustrates three consecutive positions K, K+1 and K+2 of the crawling.

3. Dynamic model for the initial phase

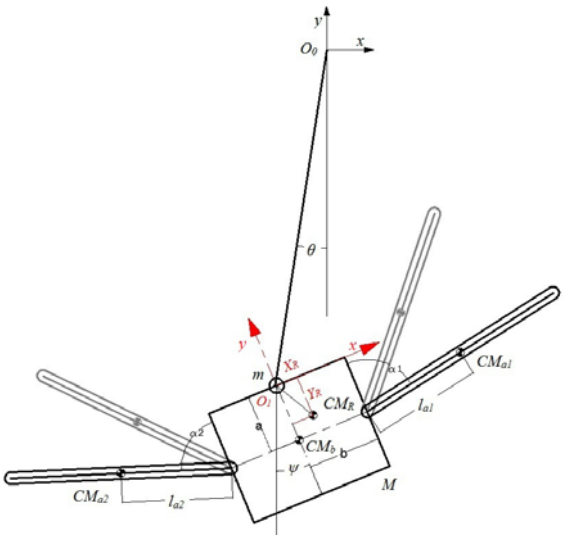

Fig. 3. Simplified model of the system

To find the equations of motions for this system (whose potential energy is time-independent), we first determine the kinetic T and potential V energy, then compute the Lagrangian $L = T - V$ and use the Euler-Lagrange equation.[3] But before applying the theory, we formulate some assumptions illustrated on Fig.3 in order to simplify the derivations:

- Due to the symmetry of the robot, central block with six uniformly

distributed arms, the robot could be represented as one platform (mass m_b), with two arms $a1$ and $a2$.

- The arms are identical with mass m and length $2l_a$.
- We consider the system as a double pendulum.
- The first pendulum consist of the inelastic cable of length l hangs from a fixed point and supports a hook of mass m.
- The simplified robot is modeled as a second pendulum with mass M, the moment of inertia I_{CM_R} and the centre of mass CM_R change while the arms are in movement.
- The motion is performed in the XY plane.

Center of mass

The center of mass changes its position due to arms' movement:

$$\overrightarrow{O_1CM_R} = \frac{m_b\overrightarrow{O_1CM_b} + m_{a1}\overrightarrow{O_1CM_{a1}} + m_{a2}\overrightarrow{O_1CM_{a2}}}{M} \quad ,$$

where $CM_R, CM_b, CM_{a1}, CM_{a2}$ are the centers of mass for the system, the platform, the first arm and the second arm respectively, and we denote $\rho = m_a/M$. The center of mass CM_r has generally coordinates

$$\begin{bmatrix} X_R \\ Y_R \end{bmatrix} = \begin{bmatrix} -\rho l_a(\sin\alpha_1 + \sin\alpha_2) \\ -a + \rho l_a(\cos\alpha_1 + \cos\alpha_2) \end{bmatrix} \quad . \tag{1}$$

In our design $l_{a1} = l_{a2} = l_a$, $m_{a1} = m_{a2} = m_a$, and we assume both arms open simultaneously: $\alpha_2(t) = -\alpha_1(t) = \alpha(t)$. Hence, the CM_R is at:

$$\begin{bmatrix} X_R \\ Y_R \end{bmatrix} = \begin{bmatrix} 0 \\ -a + 2\rho l_a \cos\alpha(t) \end{bmatrix} \tag{2}$$

Moment of inertia

The moment of inertia for the system at the center of mass CM_R is equal to the sum of the moments of inertia of the platform and two arms at CM_R.

$$I_{CM_R} = I^b_{CM_R} + I^{a_1}_{CM_R} + I^{a_2}_{CM_R} \tag{3}$$

Applying the theorem of parallel axes, the eq. (3) becomes

$$I_{CM_R} = I_{CM_b} + m_b d_b^2 + I_{CM_{a_1}} + m_{a_1} d_{a_1}^2 + I_{CM_{a_2}} + m_{a_2} d_{a_2}^2 \quad , \tag{4}$$

where $I_{CM_b}, I_{CM_{a_1}}, I_{CM_{a_2}}$ are the moments of inertia of the platform, the first arm and the second arm respectively around their own centers of mass, d_b, d_{a_1}, d_{a_2} are the distances between the center of mass for the system and the centers of mass of the platform, first and second arm respectively

$$I_{CM_R} = I_0 + k_0 + k_1\cos^2\alpha + k_2\sin\alpha \quad , \tag{5}$$

$$\text{where } I_0 = I_{CM_b} + I_{CM_{a_1}} + I_{CM_{a_2}} \qquad k_0 = 2m_a(b^2 + l_a^2)$$
$$k_1 = 4m_b\rho^2 l_a^2 + 8m_a l_a^2\rho(\rho - 1) \qquad k_2 = 2bm_a l_a$$

Equations of motion

Let θ, ψ and α are the generalized coordinates, where $\theta(t)$ is the swinging angle of the mass m, $\psi(t)$ is the tilting angle for the second pendulum, $\alpha(t)$ is the angle of opening the arms, as shown on Fig. 3. The Cartesian coordinates of m, M in the frame O_0xy expressed in terms of θ, ψ, α are:

$$x_m = l\sin\theta\ , \qquad X_M = l\sin\theta - 2\rho l_a(\cos\alpha\sin\psi) + a\sin\psi\ ,$$
$$y_m = -l\cos\theta\ , \qquad Y_M = -l\cos\theta + 2\rho l_a(\cos\alpha\cos\psi) - a\cos\psi\ .$$

Substituting and mathematical manipulating, we obtain the Lagrangian:

$$\begin{aligned} L = {} & \frac{1}{2}(m+M)(l^2\dot\theta^2) + \frac{1}{2}Ma^2\dot\psi^2 + M[2\rho^2 l_a^2(\dot\alpha^2\sin^2\alpha + \dot\psi^2\cos^2\alpha) \\ & + 2l\rho l_a\dot\theta(\dot\alpha\sin\alpha\sin(\psi-\theta) - \dot\psi\cos\alpha\cos(\psi-\theta)) + al\dot\theta\dot\psi\cos(\theta-\psi) \\ & - 2a\rho l_a\dot\psi^2\cos\alpha] + \frac{1}{2}(I_0 + k_0 + k_1\cos^2\alpha + k_2\sin\alpha)\dot\psi^2 \\ & + (m+M)gl\cos\theta - Mg(2\rho l_a\cos\alpha\cos\psi - a\cos\psi)\ . \end{aligned} \tag{6}$$

The equation of motion obtained by varying $\theta(t)$ is

$$\begin{aligned} & -(m+M)glsin\theta = (m+M)l^2\ddot\theta + aMl(\ddot\psi\cos(\theta-\psi) + \dot\psi^2\sin(\theta-\psi)) \\ & + 2Ml\rho l_a[\ddot\alpha\sin\alpha\sin(\psi-\theta) + \dot\alpha^2\cos\alpha\sin(\psi-\theta) - \ddot\psi\cos\alpha\cos(\psi-\theta) \\ & + 2\dot\alpha\dot\psi\sin\alpha\cos(\psi-\theta) + \dot\psi^2\cos\alpha\sin(\psi-\theta)]\ . \end{aligned} \tag{7}$$

The equation of motion obtained by varying $\psi(t)$ is

$$\begin{aligned} & Mg(2\rho l_a\cos\alpha\sin\psi - a\sin\psi) = Ma^2\ddot\psi - (k_1\dot\alpha\sin\alpha\cos\alpha - k_2\dot\alpha\cos\alpha)\dot\psi \\ & + M[4\rho^2 l_a^2(\ddot\psi\cos^2\alpha - 2\dot\psi\dot\alpha\sin\alpha\cos\alpha) - 2l\rho l_a(\ddot\theta\cos\alpha\cos(\psi-\theta) \\ & + \dot\theta^2\cos\alpha\sin(\psi-\theta)) + al(\ddot\theta\cos(\theta-\psi) - \dot\theta^2\sin(\theta-\psi)) \\ & - 4a\rho l_a(\ddot\psi\cos\alpha - \dot\psi\dot\alpha\sin\alpha)] + (I_0 + k_0 + k_1\cos^2(\alpha) + k_2(\sin\alpha))\ddot\psi\ . \end{aligned} \tag{8}$$

The equation of motion obtained by varying $\alpha(t)$ is

$$\begin{aligned} & M[4\rho^2 l_a^2(-\dot\psi^2\sin\alpha\cos\alpha) + \dot\psi\sin\alpha\cos(\psi-\theta)) + 2a\rho l_a\dot\psi^2\sin\alpha] \\ & + \frac{1}{2}(-2k_1\sin\alpha\cos\alpha + k_2(\cos\alpha))\dot\psi^2 + 2Mg\rho l_a\sin\alpha\cos\psi = \\ & + 4M\rho^2 l_a^2\ddot\alpha\sin^2\alpha + 2M\rho^2 l_a^2\dot\alpha^2\cos\alpha\sin\alpha \\ & + 2Ml\rho l_a(\ddot\theta\sin\alpha\sin(\psi-\theta) + \dot\theta(\dot\psi-\dot\theta)\sin\alpha\cos(\psi-\theta))\ . \end{aligned} \tag{9}$$

When the arms are steady at their final position, the effect of α vanishes from the eq.(7) and eq.(8) and they are reduced to:

$$(m+M)l\ddot{\theta} = -(m+M)g\sin\theta - aM\left[\ddot{\psi}\cos(\theta-\psi) + \dot{\psi}^2\sin(\theta-\psi)\right] \quad , \quad (10)$$

$$(I_{CM}+Ma)\ddot{\psi} + Mga\sin\psi = -Mal\left[\ddot{\theta}\cos(\theta-\psi) + \dot{\theta}^2\sin(\theta-\psi)\right] \quad . \quad (11)$$

Equations (10) and (11) describe the motion of a double pendulum.

4. Computer dynamic simulation

We use ADAMS software to simulate the real physical performance by importing the designed prototype from Inventor, introducing the corresponding connectors, forces and motion. Revolute joints between the arms and the platforms, and a contact force between the platform's shoulders and the arms were defined. The robot suspension by a cable was created by the Machinery/Cable toolkit.

The angle θ is obtained by user-defined function to measure the angle between the cable and the vertical axis Z. The ψ corresponds to the roll angle for the top platform. Due to the initial vertical pose of the arms and the gravity force the arms rotate from $\alpha = 2^\circ$ to 100°, where they stop when hitting the platform shoulders. Fig. 4 shows the variation of θ and ψ having initial conditions $\theta_0 < 1^\circ$ and $\psi_0 = 0^\circ$. The arms opening takes about 1.4 second. During this time interval the oscillation of the two angles remains too small. When arms hit the platform shoulders, they stop and the contact impacts create oscillations that are within small range of $\pm 5^\circ$.

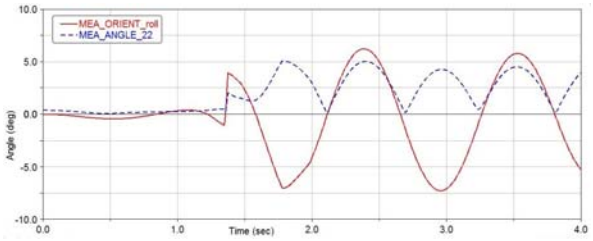

Fig. 4. The oscillation of θ and ψ when $\theta_0 < 0.5^\circ$ and $\psi_0 = 0^\circ$

Small changes in the initial conditions can force undesired system response. Fig. 5 shows the angles using initial conditions $\theta_0 = 2.5^\circ$ and

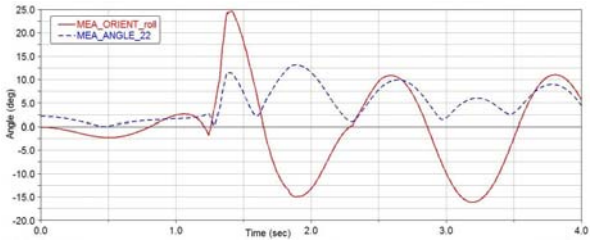

Fig. 5. The oscillation of θ and ψ when $\theta_0 = 2.5°$ and $\psi_0 = 0°$

$\psi_0 = 0°$. The amplitude of the oscillation increased to $\pm 15°$. Further increase of θ_0 beyond about 3° brings the system to chaotic but still stable swinging, which attenuates after several periods of oscillations.

When doing the same simulations, but without arms opening, i.e. considering that α is constant, there is no opening interval as existing on Fig. 4 and Fig. 5. Angle θ oscillates within a small range and the roll amplitude keeps below $\pm 5°$, as shown on Fig. 6.

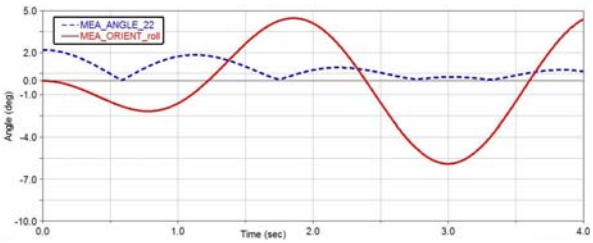

Fig. 6. The oscillation of θ and ψ when $\theta_0 = 2.5°$, $\psi_0 = 0°$ and fixed arms

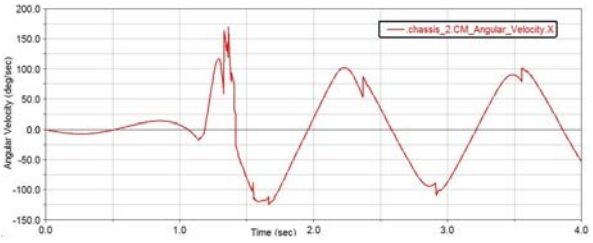

Fig. 7. Angular velocity of the top platform when $\theta_0 = 2.5°$, and $\psi_0 = 0°$

Studying the angular velocity $\dot{\psi}$ of the center of mass of the top platform

we can observe how the arms opening turns the system into a two-regime system described by two different dynamic equations - one during the arms opening, and a second after stopping at the platform shoulders. Obviously, the final conditions in the first regime become initial conditions for the second one. Fig. 7 shows that during the arms' opening $\dot{\psi}$ is almost constant. In the second part, the contact impulse appears and the value of $\dot{\psi}$ suddenly increased 10 times the value before collision.

5. Conclusion

In this paper we presented the concept of a suspended robot for cleaning of the interior surface of silos. Its design is based on minimalistic approach to achieve needed functionality, reasonable complexity and cost of the system. The foldable and expandable structure of the robot yields variable dynamical properties that requires special attention in order to guarantee stability of the motions during the entire cleaning process.

A dynamical study for the robot in suspending phase was presented, where the equations of motion were derived applying Euler-Lagrange equation. The model of the system could be used in control to eliminate the vibration. The computer simulation of the real designed robot using MSC ADAMS shows the sensitivity of the system for the initial conditions, and the effect of the arms' movement on the response of the system.

According to this study the robot is an under-actuated system unstable in the initial phase. Therefore to stabilize this system we need to activate and control the passive joints or to make the connection between the robot and the hanging point rigid.

References

1. Ju-Hwan Cha, Myung-Il Roh, and Kyu-Yeul Lee. Dynamic response simulation of a heavy cargo suspended by a floating crane based on multibody system dynamics. *Ocean Engineering*, 37(14–15):1273 – 1291, 2010.
2. K. Dandan, A. Ananiev, and I. Kalaykov. SIRO: The silos surface cleaning robot concept. In *Mechatronics and Automation (ICMA), 2013 IEEE International Conference on*, pages 657–661, 2013.
3. David Morin. *Introduction to Classical Mechanics: With Problems and Solutions*, chapter 6. Cambridge University Press, 2008.
4. Ministry of Labour. *Confined Spaces Guideline* . Occupational Health and Safety Branch, Ontario, 2009.
5. Oliver Sawodny Patrick Schlott. Decoupling control for a gantry crane with an actuated load. In *Industrial Electronics and Applications (ICIEA), 2012 7th IEEE Conference on*, pages 1610–1615, 2012.